

Cite this: *J. Mater. Chem.*, 2012, **22**, 20257

www.rsc.org/materials

PAPER

In vitro synthesis of bioactive hydroxyapatite using sodium hyaluronate as a template

Qihong Li,^a Ming Li,^a Peizhi Zhu^{*ac} and Shicheng Wei^{*ab}

Received 6th June 2012, Accepted 6th August 2012

DOI: 10.1039/c2jm33624c

Being a biocompatible and bioactive material, hyaluronic acid has great potential as a template to regulate the mineralization of hydroxyapatite (HA) nanocrystals *in vitro*. Our present study investigates the effects of sodium hyaluronate (SH) concentrations and initial pH values on the chemical composition, morphology and biological properties of hydroxyapatite (HA) crystals prepared by the wet chemical approach. All purified products were studied by Fourier transform infrared (FTIR) spectroscopy, X-ray diffractometry (XRD), X-ray photo-electronic spectroscopy (XPS), and transmission electron microscopy (TEM). This is the first time that bioactive carbonated apatites were synthesized using SH as a template. Biocompatibility of such apatites was gauged by cell vitality and alkaline phosphatase activity of MG-63 cells. The results suggested that carbonated apatites synthesized in the presence of SH were more favorable to the proliferation and differentiation of MG-63 cells compared to conventional apatites. In our study, we also found that SH temporarily stabilizes amorphous calcium phosphate (ACP) at the early stage of crystallization. The results imply that the initial pH value and the concentration of SH play a key role in affecting calcium vacancies, carbonate content and morphology of apatite crystals, as well as their effects on the proliferation and osteogenic differentiation of MG-63 cells. These synthesized carbonate-containing apatites are potentially attractive candidates for tissue engineering applications.

Introduction

Biomimetic approaches for inorganic materials synthesis can give rise to nanomaterials with improved physical and chemical properties, as well as biological properties, compared to traditional synthesis methods. Biological constituents, such as biomacromolecules, play an important role in regulating the mineralization and prevent random proliferation of crystal nuclei.¹

Based on the hypothesis that proteins regulate bone mineralization, most research efforts on bone biomimetic mineralization have focused on collagens,^{2–4} gelatin^{5,6} and peptides.^{7–9} Nudelman *et al.*⁴ even demonstrated that collagen played an active role in the formation of the oriented hydroxyapatite in bone. However, Wise *et al.*¹⁰ have recently underscored that polysaccharides, not proteins, predominantly form an organic–mineral interface. Unlike hydrophobic collagens, the functional

groups of polysaccharides can chelate Ca²⁺ ions and form hydrogen bonds with protonated PO₄^{3–} and H₂O on the surface of the mineral.¹¹ Recently, a rational biomimetic design has been shown to demonstrate that the presence of an acidic polysaccharide, maleic chitosan, stabilized the amorphous inorganic phase at the early stage of mineralization *in vitro*.¹² In addition, this study suggests that the acidic polysaccharide component plays important roles in regulating the morphology, size and crystallinity of the inorganic minerals.¹²

Hyaluronic acid is one of the largest components of the extracellular matrix (ECM), which consists of a basic unit of two sugars, glucuronic acid and *N*-acetylglucosamine, polymerised into large macromolecules. Hyaluronic acid is a natural biopolymer present in some bacterial capsules and in the intercellular matrix of vertebrate connective tissue like cartilage. Since hyaluronic acid is unstable in an acid form, it is usually extracted and refined as a sodium salt. At physiological pH, hyaluronic acid assumes the double helical form,^{13,14} which degrades with the addition of NaOH.¹⁵ It is reported that *N*-acetylglucosamine of hyaluronic acid is degraded in basic solution, and hydrolyzed at the glucuronic acid residue in acidic solution forming the hemiacetal.¹⁶ Studies have indicated that the degradation products of hyaluronic acid appear to regulate wound healing by prompting angiogenesis.¹⁷ The biocompatibility of hyaluronic acid and its key role in tissue development, repair, and function allow for wide use in clinical applications, such as regeneration,

^aCenter for Biomedical Materials and Tissue Engineering, Academy for Advanced Interdisciplinary Studies, Peking University, Beijing 100871, People's Republic of China. E-mail: sc-wei@pku.edu.cn; Fax: +86 10 62753404; Tel: +86 10 62753404

^bDepartment of Oral and Maxillofacial Surgery, Laboratory of Interdisciplinary Studies, Peking University School of Stomatology, Beijing 100081, China

^cDepartment of Chemistry, University of Michigan, Ann Arbor, Michigan 48109-1055, USA. E-mail: pzzhu@umich.edu; Fax: +1 734 7630477; Tel: +1 734 7630477

dermal scaffolds, cartilage defects, glial cell culture and spermatogenic motility assessment.

Hydroxyapatite (HA), $[\text{Ca}_{10}(\text{PO}_4)_6(\text{OH})_2]$, neither antigenic nor cytotoxic,¹⁸ is well-known as a suitable bone repair and substitute material. Its chemical composition and crystal structure are similar to the mineral in human bone and teeth,¹⁹ and is used as a raw material for the manufacture of implants and scaffolds. A large number of methods for the synthesis of apatites have already been published.^{20–22} But the synthetic apatites produced by traditional approaches usually have lower carbonate content and larger particle sizes compared to biological apatites. Currently, researchers are concentrating on synthesizing carbonated apatites with specific morphologies and nano-scale sizes to more closely resemble biological apatites.²³

The human osteosarcoma cell line MG-63 belongs to a particular subpopulation of osteoblasts, namely, osteoblast precursors or early undifferentiated osteoblast-like cells.²⁴ The sequential expression of genes for collagen type I and alkaline phosphatase (ALP), which is characteristic of osteoblast differentiation, features MG-63 differentiation.^{25,26} MG-63 cells have been widely used to decide whether a material is biocompatible and promotes osteogenic differentiation.^{27,28}

The negatively charged groups on hyaluronic acid and its hydrolytic products play an important role in regulating the mineralization of apatites, because they have a high affinity for calcium ions in solution and can prevent crystals from aggregation. The purpose of this study was to address the effects of the concentration of SH and the initial pH value on the chemical compositions, morphology and biological properties of apatites synthesized by the chemical precipitation method. All products were characterized by Fourier-transform infrared (FTIR) spectroscopy, X-ray diffractometry (XRD), X-ray photo-electronic spectroscopy (XPS), and transmission electron microscopy (TEM). The impacts of as-prepared samples on the proliferation and osteogenic differentiation of MG-63 cells have been evaluated by CCK-8 and alkaline phosphate activity assay.

Experimental

Materials

$\text{Ca}(\text{NO}_3)_2 \cdot 4\text{H}_2\text{O}$ (AR, Tianjin, China), $(\text{NH}_4)_2\text{HPO}_4$ (AR, Beijing, China), HNO_3 (AR, Hebei, China), $\text{NH}_3 \cdot \text{H}_2\text{O}$ (AR, Tianjin, China), and sodium hyaluronate (>1000 kDa, Shanghai, China) were used as received without further purification.

Synthesis of carbonated apatites

The synthesis procedure for apatites under atmospheric conditions includes heating of an aqueous mixture of $\text{Ca}(\text{NO}_3)_2$ and $(\text{NH}_4)_2\text{HPO}_4$ at 95 °C for 4–6 h. SH was added as a template at the concentrations of 0, 1.5, 10 and 30 mg ml⁻¹. The specific synthetic conditions of each sample are listed in Table 1. Solution pH was carefully adjusted from the initial pH of 2 by adding $\text{NH}_3 \cdot \text{H}_2\text{O}$. The resultant white solution was aged at ambient temperature overnight. The products were washed at least three times with deionized water until impurities were completely removed, then dried in an oven at 60 °C before characterization.

Synthesis of early stage products

At the room temperature, ammonium dibasic phosphate solution [$(\text{NH}_4)_2\text{HPO}_4$, 50 ml, 0.2 mol l⁻¹] was rapidly poured into stirred calcium nitrate solution [$\text{Ca}(\text{NO}_3)_2 \cdot 4\text{H}_2\text{O}$, 50 ml, 0.334 mol l⁻¹] with 0.3 g per 100 ml of SH. Before mixing, the pH values of both solutions mentioned above were adjusted to 10 by adding $\text{NH}_3 \cdot \text{H}_2\text{O}$. Immediately after precipitation the suspension was filtered and washed with icy deionized water and finally lyophilized for 72 h. Precipitations were also collected after reaction for 600 s, 1200 s and 1800 s. For comparison, the early stage powders prepared in the absence of SH were also obtained as the control group.

Measurements

The crystalline powders were identified and analyzed by X-ray diffraction (XRD, Standard attachment XRD 6000, Shimadzu, Tokyo, Japan). Fourier transform infrared spectrometry (FTIR, Magna-IR 750, Nicolet, USA) was used to detect samples which were in the form of pellets (KBr pellet). The chemical constituents were analyzed by X-ray photo-electronic spectroscopy (XPS, Kratos, UK). Microstructural characterization was carried out using a Tecnai F30 transmission electron microscope (TEM). Selected Area Electron Diffraction (SAED) was recorded using the same equipment.

Cell proliferation

Human osteoblast-like cell line MG-63 cells (American Type Culture Collection, VA, USA) were cultured in α -MEM medium (Invitrogen) supplemented with 10% of fetal calf serum (FCS), 100 $\mu\text{g ml}^{-1}$ penicillin and 100 $\mu\text{g ml}^{-1}$ streptomycin in a humidified atmosphere with 5% CO_2 at 37 °C. After cell counting, MG-63 cells were seeded in 96-well culture plates (Costar, USA) at a density of 5×10^3 cells per well for proliferation and differentiation assays.

The impact of the prepared samples on the proliferation of human osteoblast-like MG-63 cell line was evaluated by a cell counting kit-8 assay (CCK-8, Dojindo). One day after seeding, cells were rinsed with phosphate-buffered saline (PBS) and exposed to different samples with the concentration of 20 $\mu\text{g ml}^{-1}$. The culture medium was refreshed with α -MEM every 2 days. After co-culture for one day, three days and five days, 10 μl of CCK-8 was added into each well and incubated for 4 h. Then 80 μl of supernatant from each well was transferred to new 96-well cell culture dishes. Optical density (OD) measurements were performed using a spectrophotometer (Elx-800, bio-Tek instruments) at 450 nm, with a reference wavelength of 630 nm.

Alkaline phosphate activity assay

Alkaline phosphatase (ALP) activity of MG-63 cells was assayed by a test kit (Nanjing Jiancheng Bioengineering Institute, China). Free phenol, which is produced in the hydrolysis process of *p*-nitro-phenyl phosphate (*p*-NPP) with ALP acting as a catalyst, reacts with 4-amino-antipyrine to form a red-coloured complex. The absorbance of such a complex measured at 520 nm is proportional to the ALP activity in the samples. Briefly, after co-culturing as-prepared samples and MG-63 for 7 days, the

Table 1 Synthesizing conditions for preparing carbonated apatites with SH as a template

Sample name	SH (g per 100 ml)	[Ca ²⁺] (mol l ⁻¹)	[PO ₄ ³⁻] (mol l ⁻¹)	Time (h)	T (°C)	pH value
Pure HA	0	0.167	0.1	4	95	2 → 10
pH2T015	0.15	0.167	0.1	4	95	2 → 10
pH2T1	1	0.167	0.1	4	95	2 → 10
pH2T3	3	0.167	0.1	4	95	2 → 10
pH10T015	0.15	0.167	0.1	4	95	10
pH74T015	0.15	0.167	0.1	6	95	7.4 → 10

supernatant was removed and 100 μl of lysis solution (1% TritonX-100) was added into each well and incubated for 1 h. Afterwards, 30 μl of MG-63 cell lysates at each well was transferred to new 96-well cell culture dishes, and cultivated with 50 μl of carbonated buffer solution (pH = 10) and 50 μl of substrate solution (4-amino-antipyrine) at 37 °C for 15 min. Then 150 μl of potassium ferricyanide (a chromogenic agent) was added into the above solution and its absorbance was measured at the wavelength of 520 nm by a spectrophotometer (Elx-800, bio-Tek instruments). For normalization, the total protein concentration was measured by a bicinchoninic acid (BCA) protein assay kit (Beijing Biosea Biotechnology, China). Thus the ALP activity was normalized and expressed as the total protein content (U per g prot.). Each experiment was performed in triplicate for each group and repeated twice to get similar results at least.

Statistical analysis

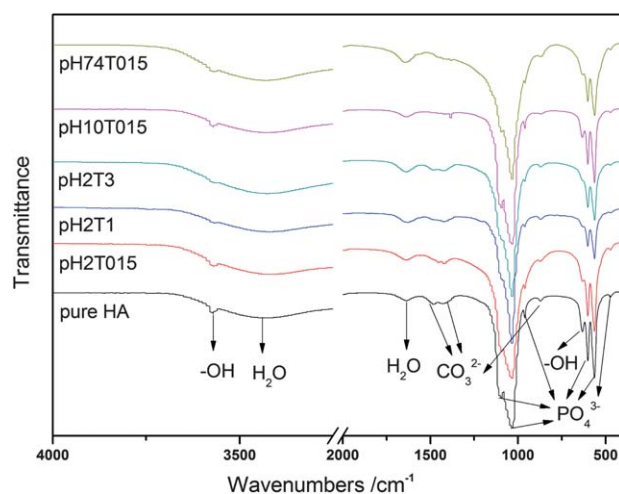
All quantitative data expressed as mean ± standard deviations are derived from experiments carried out in triplicate. Statistical analysis was carried out with Origin software. Student's *t*-test was used to identify the significant differences among the experimental groups, and a *p*-value of <0.05 was considered statistically significant.

Results and discussions

Fourier transform infrared spectroscopy

The FTIR spectra of all as-prepared powders are shown in Fig. 1. Both the intense peak at 3570 cm⁻¹ and the weak peak at 632 cm⁻¹ belong to the stretching (ν_s) and vibrational modes (ν_L) of the hydroxyl anions, which usually exist in the HA crystal.²⁹ The broad peaks, at approximately 3428 and 1633 cm⁻¹, should be assigned to the adsorbed water within HA.³⁰ The weak bands, which are detected at about 1459, 1417 and 872 cm⁻¹, indicate that there is a partial substitution of CO₃²⁻ for PO₄³⁻ (B-type).^{31,32} The bands at around 1095 and 1039 cm⁻¹ are likely attributed to the triply degenerate ν_3 antisymmetric P–O stretching modes, and the peak at 962 cm⁻¹ is assigned to the ν_1 non-degenerate symmetric P–O bond stretching band. Additionally, the peaks at about 602 and 570 cm⁻¹ should belong to the triply degenerate ν_4 vibration of O–P–O bonds³³ and the peak at nearly 433 cm⁻¹ is attributed to the ν_2 of the P–O mode.^{34,35}

The spectra of the samples synthesized by adding SH into the solution are very similar to that of pure HA, even though there are still some differences, which are clearly shown in Table 2. It is easily found that as the SH concentration is increased, the ν_3 and ν_1

**Fig. 1** FTIR spectra of as-synthesized carbonated apatites under different conditions. The FTIR spectrum of pure HA is shown for reference.

vibrations of P–O bonds, as well as the ν_3 and ν_L vibrations of the hydroxyl anions, could not be detected. It may be ascribed to more substitution of carbonate for both PO₄³⁻ and OH⁻, which are called B-type and A-type substitutions, respectively.³⁶ Compared to pH2T015, ν_3 and ν_1 vibrations of P–O bonds are hardly detected in pH74T015, as well as the CO₃²⁻ vibration in pH10T015.

X-ray diffraction studies

XRD patterns of the six synthesized samples are shown in Fig. 2. The diffraction peaks of the products prepared by SH agree with those of pure HA at 2θ values of 25.9°, 31.8°, 32.9°, 39.8°, 46.7°, 49.5° and 53.1°, which are indexed to (002), (211), (300), (310), (222), (213) and (004) planes, respectively.³⁷ The intense bands at around $2\theta = 26^\circ$ and $2\theta = 33^\circ$ demonstrate that the samples are predominantly HA.

As the SH concentration is increased the diffraction peaks, in particular the three most intense peaks of HA [corresponding to (211), (112), and (300) planes], become broader, which indicates that the dimension of the apatite nanocrystals is decreased.³⁸ The patterns of carbonated apatites with broader bands are very similar to those of minerals in human bone and dentin.³⁹ In addition, with the same SH concentration, the low initial pH value (pH = 2) contributes to the product with sharp peaks. However, both neutral and alkaline solutions lead to the production of apatite crystals with broader bands, which may be ascribed to smaller sized crystals.

Table 2 The different categories of specific functional groups existing in as-prepared samples

	OH ⁻ at 3570 and 632 cm ⁻¹	CO ₃ ²⁻ (B type) at 1459, 1417 and 872 cm ⁻¹	PO ₄ ³⁻ (ν_3) at 1095 cm ⁻¹	PO ₄ ³⁻ (ν_1) at 962 cm ⁻¹
Pure HA	✓	✓	✓	✓
pH2T015	✓	✓	✓	✓
pH2T1	×	✓	×	×
pH2T3	×	✓	×	×
pH10T015	✓	×	✓	✓
pH74T015	✓	✓	×	×

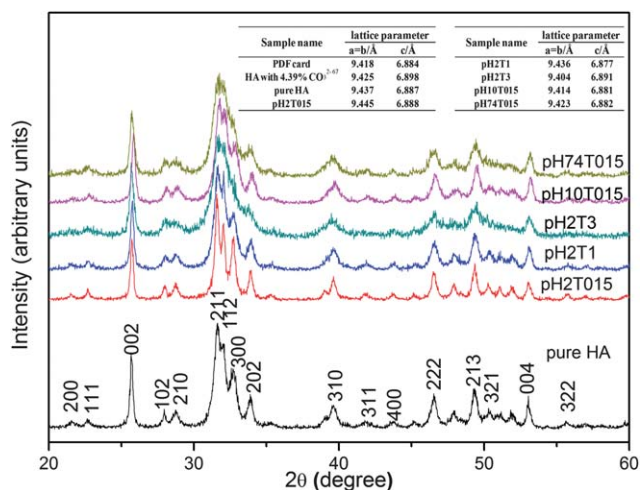


Fig. 2 XRD patterns of as-prepared apatites under different conditions. The diffraction pattern of pure HA is shown for reference.

The unit cell parameters for apatites obtained were also calculated. The lattice parameters for calcium hydroxyapatite were reported to vary between 9.403 and 9.49 Å for the *a* axis and between 6.866 and 6.940 Å for the *c* axis.^{40–42} Additionally, the lattice dimensions vary with the A-type carbonate content.^{43,44} The *a* dimension systematically increases and the *c* dimension decreases with increasing carbonate content. The dimensions of an A-type carbonated apatite containing 4.4% CO₃²⁻ (A-type) were used for reference.⁴⁵ The order of A-type carbonate content in as-prepared apatites is as follows: pH2T015 > pure HA ≥ pH2T1 > pH74T015 > pH10T015 > pH2T3. The lattice dimensions of pH10T015 are almost equivalent to the standard ones (PDF # 72-1243), which indicates that there is no A-type carbonate in this sample.

X-ray photoelectron spectroscopy

X-ray photoelectron spectroscopy, an important surface analytical tool widely used in the field of biomaterials, was applied to examine as-prepared hydroxyapatite powders for the calcium to phosphorous ratio and also for identifying the presence of impurities. The XPS wide scan shows that calcium, phosphorus, oxygen and small amounts of carbon elements were present in the reference sample, whose spectrum is in agreement with a previous report (Fig. 3).⁴⁶ Other products studied have the same typical characteristics as the reference sample. The Ca/P ratios of all samples, which are very close, are less than 1.67, indicating the calcium-deficient state on the HA crystalline surface.

Moreover, the analysis of the elementary composition (Table 3) shows that with the increase of SH concentration, the carbon element content in the products synthesized at the same initial pH value is also raised. It illustrates that the solution system with more hydrolytic products may lead to more CO₂ absorption. Additionally, the products synthesized at the same SH concentration have distinct carbon element contents, and their sequence in the carbon element content is as follows: pH2T015 > pH74T015 > pH10T015. This implies that when hydrolytic products mainly function as templates to guide the growth of HA crystals, the CO₃²⁻ substitution in HA is inhibited. FTIR and

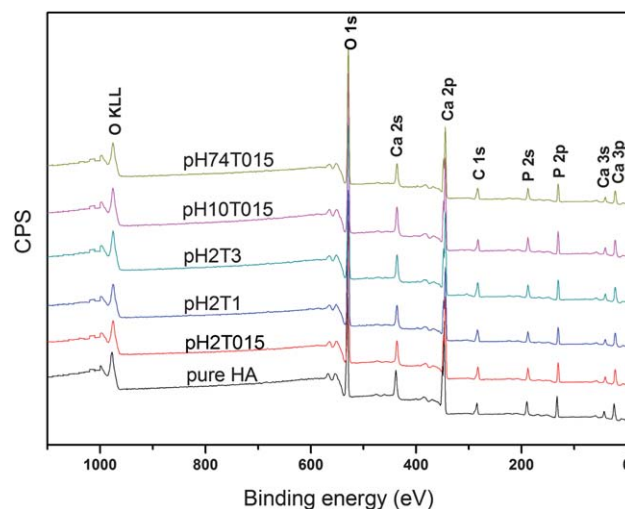


Fig. 3 XPS spectra of as-synthesized apatites under different conditions. The XPS survey spectrum of pure HA is shown for reference.

XRD analyses identified that there were no A-type and B-type carbonate substitutions in pH10T015, the carbon element detected in the sample may be due to carbon contamination in the detector. Nitrogen was not detected in all the as-prepared powders, illustrating that there are no presence of any organic residuals. These results are in agreement with the FTIR analysis.

Morphology analysis using TEM

Fig. 4 shows TEM micrographs of the as-synthesized samples, from which it was easily seen that the pure HA featured very irregular morphology. The morphology of pH2T1 is sharply different from that of pure HA. It indicates that the presence of hydrolytic products of SH in solution may interfere with the growth of carbonated apatite crystals, even though those hydrolytic pieces could not be able to attract calcium ions at a low pH value and nucleation of apatites could mainly occur in solution. It was also observed that with the increase of the SH concentration, the morphology of apatite crystals changes greatly. It illustrates that more hydrolytic products lead to bigger steric hindrance, which seriously disturbs the growth of carbonate-containing apatite crystallines. Both pH74T015 and pH10T015 have similar rod-like morphologies, which are very different from that of pH2T015. However, the rods of pH10T015 are more uniform than those of pH74T015, because the length of hydrolytic products at a constant pH value of 10 is more even. Under alkaline conditions, those hydrolytic pieces function as templates to attract calcium ions, promote nucleation of minerals and guide the growth of crystals along the chains.

Table 3 Elementary composition of the as-synthesized apatites

	Ca (At%)	P (At%)	O (At%)	C (At%)	Ca/P ratio
Pure HA	21.42	15.29	49.26	14.03	1.40
pH2T015	19.83	15.11	48.02	17.04	1.31
pH2T1	18.88	13.91	49.80	17.41	1.36
pH2T3	18.94	14.30	49.13	17.63	1.32
pH10T015	20.88	16.10	50.02	13.00	1.30
pH74T015	18.70	14.79	50.75	15.77	1.26

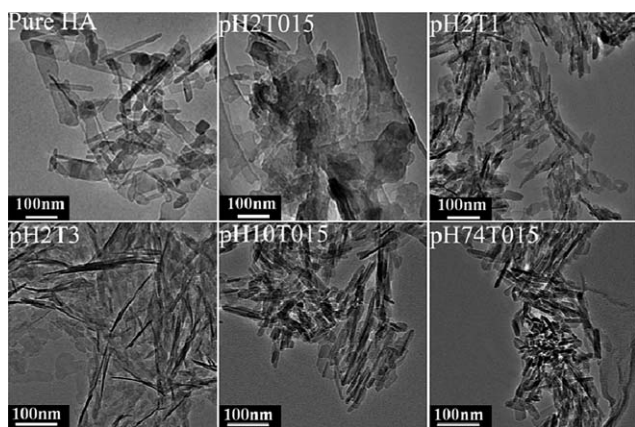


Fig. 4 TEM micrographs of all carbonated apatites prepared under different conditions. The image of pure HA is shown for reference.

Energy dispersive X-ray

EDX analysis in Fig. 5 and Table 4 revealed a difference in the Ca/P ratio among the as-prepared crystals. These ratios differed from those calculated by XPS, but in a similar order. This is because XPS can only investigate the surface of samples. It is found that pure HA, pH2T1 and pH2T3 have nearly the same Ca/P ratio, but that of pH2T015 is relatively low. It implies that low SH concentration under the low initial pH conditions may not contribute to production of apatites with high Ca/P ratio. In addition, at the same SH concentration, the Ca/P ratio sequence of samples is as follows: pH2T015 \leq pH74T015 < pH10T015. This indicates that the alkaline conditions may be good to aggregation of calcium ions on the $-\text{COO}-$ groups of the templates and thus contribute to the synthesis of apatites with high Ca/P ratio.

MG-63 cell vitality

The *in vitro* biocompatibility of the prepared samples was investigated using CCK-8 assay on MG-63 cell line. The viable cell number is directly proportional to the amount of CCK-8 assay products, formazan, which shows a linear response at 570 nm

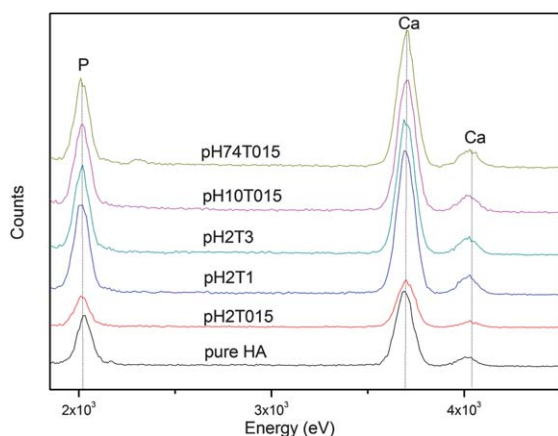


Fig. 5 TEM-associated EDX area analysis of the as-prepared powders prepared under different conditions. The pattern of pure HA is shown for reference.

Table 4 Calcium to phosphate ratio derived from EDX patterns of the as-synthesized powders

	Pure HA	pH2T015	pH2T1	pH2T3	pH10T015	pH74T015
Ca	60.191	58.521	60.802	61.149	62.665	59.009
P	39.808	41.478	39.197	38.85	37.334	40.99
Ca/P ratio	1.51	1.41	1.55	1.57	1.67	1.44

absorbance values. From Fig. 6, it can be seen that the viability of MG-63 cells incubated with each sample ($20 \mu\text{g ml}^{-1}$) for 1 day displays little statistical differences with that of the control group. While, after 3 days incubation, pH2T1, pH2T3 and pH10T015 groups show lower absorbance than the control group, but higher than the other three groups (pure HA, pH2T015 and pH74T015 groups). Similar results are obtained after 5 days incubation. However, the pH2T1 and pH10T015 groups presented little statistical difference with the control group. Therefore, the inhibitory effect of the samples on the MG-63 growth after 5 days incubation is as follows: pure HA > pH74T015 \approx pH2T015 > pH2T3 \approx pH10T015 \approx pH2T1. The distinct 570 nm absorbance could be ascribed to the difference in the morphology, carbonate content and the Ca/P ratio of the synthesized nano-apatite crystals. It is reported that the crystals of biological apatite are always of a small size⁴⁷ and that the substitution of carbonate can increase the lattice strain of HA and enhance its solubility, which makes HA biologically active.⁴⁸ In addition, calcium-deficient apatites are also of biological importance^{49,50} since the catalytic activity of HA is proportional to the calcium deficiency⁵¹ of the sample. Large amounts of carbon, non-stoichiometric Ca/P ratio and appropriate nano-morphology may be the co-contributors to the biocompatibility of apatites.

Properties of all as-prepared samples are listed in Table 5, from which it is observed that cells co-cultured with pH10T015 display very good vitality. pH2T1 also features good biocompatibility derived from its small size, low Ca/P ratio as well as large amounts of carbonate substitution. pH2T3 also results in good cell vitality due to its low Ca/P ratio, large amounts of carbon and appropriate morphology of crystals. However, both pH2T015 and pH74T015 led to very poor biocompatibility

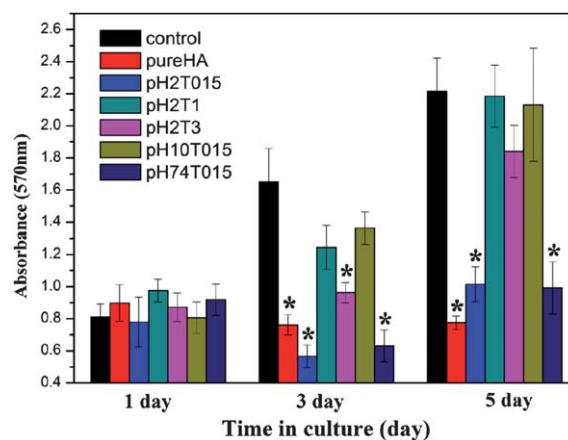


Fig. 6 *In vitro* cytotoxicity of MG-63 cell lines after culturing with the prepared samples for 1 day, 3 days and 5 days. * represents $p < 0.05$ compared with the control groups.

Table 5 Properties of all as-synthesized carbonated apatite samples

	Carbon (At%)	Ca/P ratio	Morphology
Pure HA	14.03	1.51	Irregular
PH2T015	17.04	1.41	Cloud-like
PH2T1	17.41	1.55	Flake-like
PH2T3	17.63	1.57	Sheet-like
PH10T015	13.00	1.67	Rod-like ^a
PH74T015	15.77	1.44	Rod-like ^b

^a 52.6 ± 8.8 nm, 15.8 ± 3.5 nm. ^b 41.8 ± 5.5 nm, 18.2 ± 5.5 nm.

mainly due to its very low Ca/P ratio, making the crystals too chemically active. Pure HA features irregular morphology which has little biological activity.

Alkaline phosphatase activity

For the purpose of investigating the impact of these morphologically unique synthetic apatites on the differentiation of MG-63 cells in culture, alkaline phosphatase (ALP) activity was measured after co-culturing with the samples. This assay is able to show early osteoblastic phenotypic expressions⁵² since alkaline phosphate is expressed in large amounts in the differentiation phase of osteoblast cells, which is indicative of osteogenesis. As shown in Fig. 7, after co-culturing for 7 days, the as-synthesized samples promote differentiation in the MG-63 in the following order: pH2T1 ≥ pH10T015 > pH2T3 ≈ pH2T015 ≈ pH74T015 > pure HA. This sequence agrees quite well with that of the inhibitory effect of these samples on the MG-63 viability after co-culturing for 5 days. This result implies that the prepared HA powders with different chemical compositions and morphologies have very similar impacts on the growth and osteogenic differentiation of MG-63 cells.

Possible synthesis mechanism for carbonated apatites crystallization

Bone sialoprotein (BSP), a polyanionic protein, has been confirmed to play a role in inducing the formation of HA. The

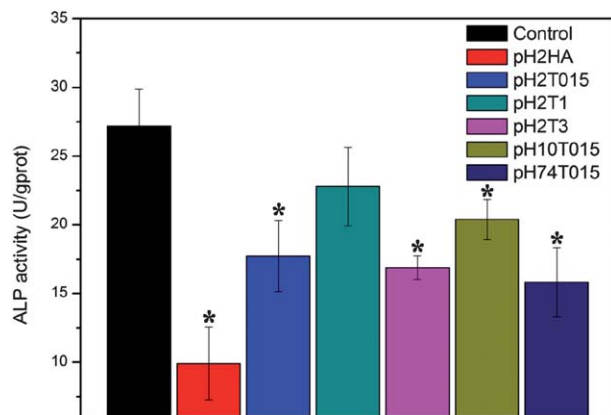


Fig. 7 ALP activity of MG-63 cell lines after culturing with the prepared samples for 7 days. * represents $p < 0.05$ compared with the control group.

glutamic acid-rich sequences of BSP are suggested to be of special importance in the nucleation of HA. Hyaluronic acid has a very similar structure with these glutamic acid-rich sequences, since both have abundant carboxyl groups.⁵³ In addition, Duer *et al.* reported that the coexistence of biomacromolecules, especially glycosaminoglycan (GAG), plays a key role in the formation of kidney stone, in which apatites predominate.⁵⁴

In this study, in order to understand how SH plays a role in HA crystallization, we analyzed the early stage products prepared at the room temperature with the addition of SH.

XRD phase identification of early stage products

Fig. 8 shows the phase transformation process of the early stage products in pH10T015 and its control group with the increase of reaction time. The initial precipitations of both pH10T015 and the control group were amorphous calcium phosphate (ACP) with a characteristic bump whose maximum was located at around $2\theta = 30^\circ$,⁵⁵ and ACP was widely recognized as the precursor for apatites formation both *in vivo*^{56–58} and *in vitro*.¹² After 600 s reaction, the diffraction peaks assigned to apatitic calcium phosphate (AP-CaP)⁵⁹ were first observed in pH10T015, which were also detected in the control group after 1800 s reaction time.

FTIR analysis results of early stage products

FTIR analysis was further used to verify the XRD results in Fig. 8. As shown in Fig. 9, the wide absorbance bands of all the samples at 3428 cm^{-1} and 1633 cm^{-1} are assigned to the absorbed water within the prepared samples.³⁰ The broad and relatively symmetrical bands of PO_4^{3-} at 1050 cm^{-1} and 560 cm^{-1} originate from ACP.⁶⁰

But with the increase of reaction time, the two peaks at 1050 cm^{-1} and 560 cm^{-1} are split into four characteristic absorbance bands approximately at 1093 cm^{-1} , 1032 cm^{-1} , 602 cm^{-1} and 562 cm^{-1} , respectively. And these four peaks are likely attributed to the acid phosphate groups in typical poorly crystalline apatitic calcium phosphate, which are similar to those

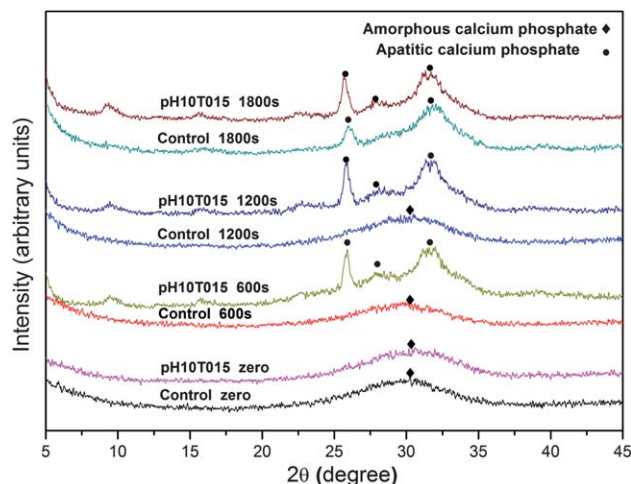


Fig. 8 XRD patterns of early stage products at different reaction times.

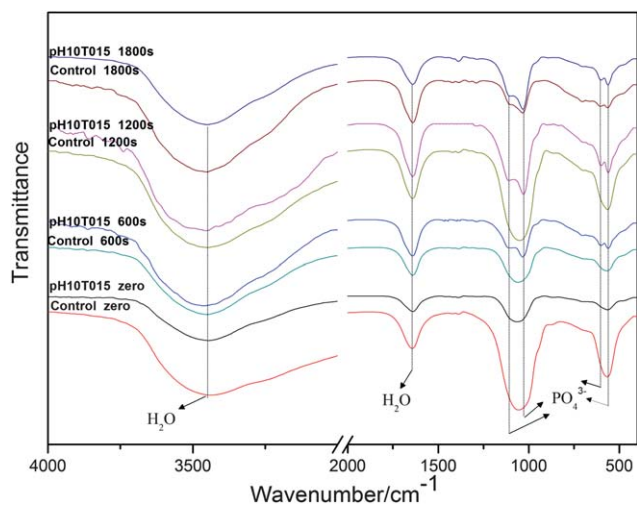


Fig. 9 FTIR spectra of early stage products at different reaction times.

Table 6 The difference of PO_4^{3-} absorbance bands shape in the samples

Group	Reaction time	Absorbance bands shape of PO_4^{3-}	
		Symmetrical	Split
Control	Zero	✓	×
	600 s	✓	×
	1200 s	✓	×
	1800 s	×	✓
pH10T015	Zero	✓	×
	600 s	×	✓
	1200 s	×	✓
	1800 s	×	✓

of HA crystalline.⁶⁰ The difference of PO_4^{3-} absorbance bands shape from 1100 cm^{-1} to 560 cm^{-1} is summarized in Table 6, and the results agree well with the XRD analysis.

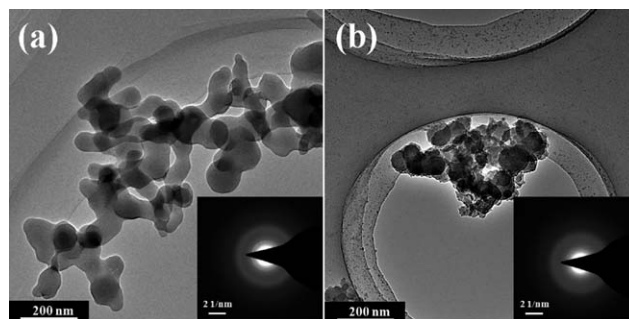
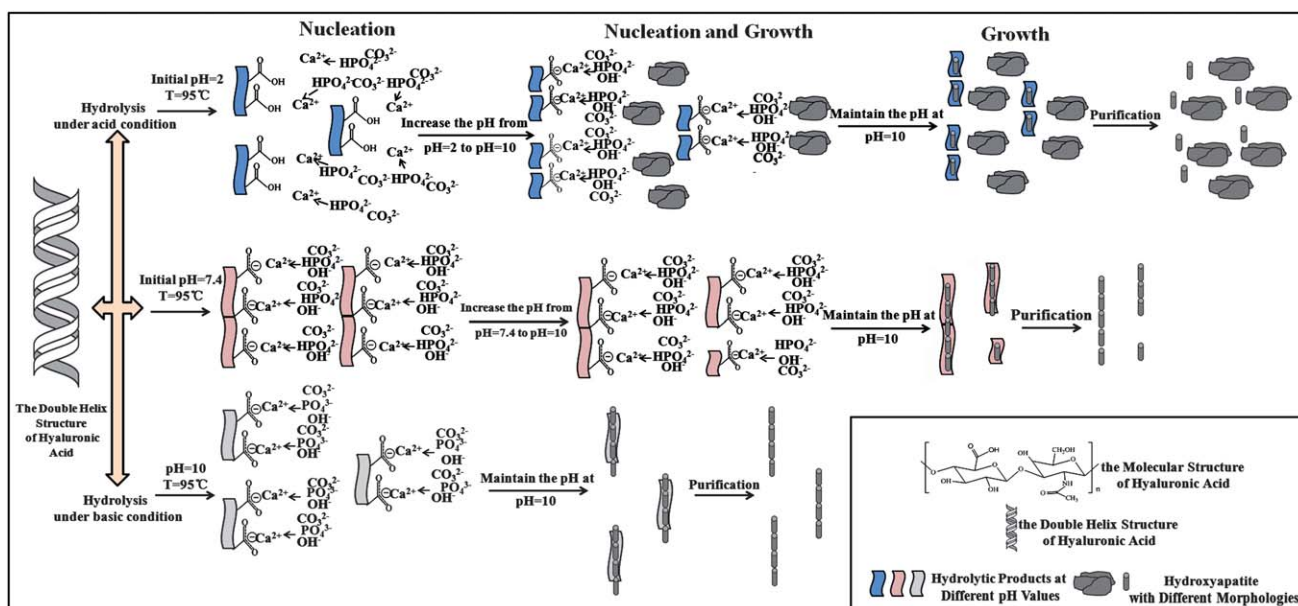


Fig. 10 TEM images of early stage products after immediate precipitation. (a: control group; b: pH10T015).

TEM images of early stage products

Products obtained after immediate precipitation were further identified by TEM and SAED. As shown in Fig. 10, spherical nanoparticles were found in both pH10T015 and the control group. The appearance of diffuse rings in the SAED pattern confirmed their amorphous feature. The amorphous characteristics were also supported by XRD data. From the TEM images, it was easily found that the amorphous particles produced in the presence of SH were smaller than those prepared without SH. This implies that at the early stage of crystallization SH may chelate with the Ca^{2+} ions on the surface of ACP, inhibit the growth of ACP nanoparticles and temporarily stabilize ACP particles through carboxyl groups in SH. The smaller nanoparticles tend to transform into more stable mineral phase with shorter induction time.^{61,62} Thus SH also facilitates the transformation of ACP to HA.

Hyaluronic acid in solution assumes a stiffened helical configuration at physiological pH, which can be ascribed to hydrogen bonding along the chain.^{13,14} The possible mechanism is shown in Scheme 1.



Scheme 1 Schematic drawings of the hydroxyapatite formation mechanism in solution with SH.

Under acid conditions, hyaluronic acid undergoes acidic hydrolysis and its unbranched long chain is broken down into pieces.¹⁶ These small pieces with –COOH groups cannot chelate calcium ions, thus the nucleation of inorganic minerals mostly goes on in solution before the pH is increased. As the acid solution becomes more alkaline, these pieces continue to undergo hydrolysis and become smaller.¹⁶ The smaller pieces with –COO[–] could chelate the remaining Ca²⁺ and further promote the nucleation of minerals. After adequate aging time, crystals grown in solution become flake-like, but the ones grown on the surface of hydrolytic products have rod-like morphology. These rods could have been covered by apatite flakes and not easily seen.

Slowly increasing the pH of neutral solution to 10 induces partial alkaline hydrolysis in the natural polymer, which leads to the production of hydrolytic pieces with different lengths. The hydrolytic products with –COO[–] easily chelate Ca²⁺, and thus form ionic clusters for the nucleation of minerals. Rod-like inorganic crystals grow on the surface of hydrolytic products, which function like a natural template.

While maintaining a pH of 10, SH undergoes alkaline hydrolysis completely, which leads to the formation of uniform hydrolytic pieces with –COO[–]. These similarly sized templates could contribute to the production of uniform apatite crystals with rod-like morphology. Changing the pH value and SH concentration in the synthesis process could lead to the production of apatites with different Ca/P ratios and carbonate contents, as well as distinct morphologies. As the biological properties of apatites largely depend on their Ca/P ratio, carbonate substitution and morphology, sodium hyaluronate appears to be an adequate template for obtaining bioactive HA.

Conclusion

The effects of the SH concentration and the initial pH value on the chemical composition, morphology, and biocompatibility of as-synthesized apatites were investigated by the chemical precipitation method for the first time. It was found that non-stoichiometric, carbonated apatites with high purity were obtained and some of them were more favorable to the proliferation and differentiation of MG-63 cells compared to HA powders synthesized without SH. The results also suggest that SH temporarily stabilizes ACP at the early stage of crystallization. The initial pH value and the concentration of SH play a key role in affecting the Ca/P ratio, carbonate content and morphology of carbonated apatite crystals, as well as their effects on the proliferation and osteogenic differentiation of MG-63 cells.

Acknowledgements

This work was supported by State Key Development Program for Basic Research of China (grant 2007CB936103), the Fundamental Research Funds for the Central Universities, and Peking University's 985 Grant.

Notes and references

1 H. Cölfen, *Nat. Mater.*, 2010, **9**, 960–961.

2 G. Falini, M. Gazzano and A. Ripamonti, *J. Mater. Chem.*, 2000, **10**, 535–538.

- 3 Y. Liu, N. Li, Y. P. Qi, L. Dai, T. E. Bryan, J. Mao, D. H. Pashley and F. R. Tay, *Adv. Mater.*, 2011, **23**, 975–980.
- 4 F. Nudelman, K. Pieterse, A. George, P. H. H. Bomans, H. Friedrich, L. J. Brylka, P. A. J. Hilbers, G. de With and N. A. J. M. Sommerdijk, *Nat. Mater.*, 2010, **9**, 1004–1009.
- 5 E. V. Rosseeva, J. Buder, P. Simon, U. Schwarz, O. V. Frank-Kamenetskaya and R. Kniep, *Chem. Mater.*, 2008, **20**, 6003–6013.
- 6 X. H. Liu, L. A. Smith, J. Hu and P. X. Ma, *Biomaterials*, 2009, **30**, 2252–2258.
- 7 M. Gungormus, M. Branco, H. Fong, J. P. Schneider, C. Tamerler and M. Sarikaya, *Biomaterials*, 2010, **31**, 7266–7274.
- 8 J. D. Hartgerink, E. Beniash and S. I. Stupp, *Science*, 2001, **294**, 1684–1688.
- 9 A. Mata, Y. B. Geng, K. J. Henrikson, C. Aparicio, S. R. Stock, R. L. Satcher and S. I. Stupp, *Biomaterials*, 2010, **31**, 6004–6012.
- 10 E. R. Wise, S. Maltsev, M. E. Davies, M. J. Duer, C. Jaeger, N. Loveridge, R. C. Murray and D. G. Reid, *Chem. Mater.*, 2007, **19**, 5055–5057.
- 11 P. Z. Zhu, J. D. Xu, N. Sahar, M. D. Morris, D. H. Kohn and A. Ramamoorthy, *J. Am. Chem. Soc.*, 2009, **131**, 17064–17065.
- 12 C. Zhong and C. C. Chu, *J. Mater. Chem.*, 2012, **22**, 6080–6087.
- 13 J. Necas, L. Bartosikova, P. Brauner and J. Kolar, *Vet. Med.*, 2008, **53**, 397–411.
- 14 I. C. M. Dea, R. Moorhouse, D. A. Rees, S. Arnott, J. M. Guss and E. A. Balazs, *Science*, 1973, **179**, 560–562.
- 15 S. Ghosh, I. Kopal, D. Zanette and W. F. Reed, *Macromolecules*, 1993, **26**, 4685–4693.
- 16 Y. Tokita and A. Okamoto, *Polym. Degrad. Stab.*, 1995, **48**, 269–273.
- 17 D. C. West, I. N. Hampson, F. Arnold and S. Kumar, *Science*, 1985, **228**, 1324–1326.
- 18 K. J. L. Burg, S. Porter and J. F. Kellam, *Biomaterials*, 2000, **21**, 2347–2359.
- 19 A. Ruksudjarit, K. Pengpat, G. Rujijanagul and T. Tunkasiri, *Curr. Appl. Phys.*, 2008, **8**, 270–272.
- 20 J. S. Earl, D. J. Wood and S. J. Milne, *J. Phys. Conf. Ser.*, 2006, **26**, 268–271.
- 21 K. P. Sanosh, M. C. Chu, A. Balakrishnan, Y. J. Lee, T. N. Kim and S. J. Cho, *Curr. Appl. Phys.*, 2009, **9**, 1459–1462.
- 22 M. A. Giardina and M. A. Fanovich, *Ceram. Int.*, 2010, **36**, 1961–1969.
- 23 R. Z. LeGeros, *Monogr. Oral. Sci.*, 1991, **15**, 1–201.
- 24 S. Grampp, H. K. Genant, A. Mathur, P. Lang, M. Jergas, M. Takada, C. C. Glüer, Y. Lu and M. Chavez, *J. Bone Miner. Res.*, 1997, **12**, 697–711.
- 25 G. S. Stein and J. B. Lian, *Endocr. Rev.*, 1993, **14**, 424–442.
- 26 D. Lajeunesse, C. Frondoza, B. Schoffield and B. Sacktor, *J. Bone Miner. Res.*, 1990, **5**, 915–922.
- 27 T. Yoshida, M. Kikuchi, Y. Koyama and K. Takakuda, *J. Mater. Sci.: Mater. Med.*, 2010, **21**, 1263–1272.
- 28 Y. C. Huang, P. C. Hsiao and H. J. Chai, *Ceram. Int.*, 2011, **37**, 1825–1831.
- 29 S. Koutsopoulos, *J. Biomed. Mater. Res.*, 2002, **62**, 600–612.
- 30 R. N. Panda, M. F. Hsieh, R. J. Chung and T. S. Chin, *J. Phys. Chem. Solids*, 2003, **64**, 193–199.
- 31 B. O. Fowler, *Inorg. Chem.*, 1974, **13**, 194–207.
- 32 Q. J. He, Z. L. Huang, Y. Liu, W. Chen and T. Xu, *Mater. Lett.*, 2007, **61**, 141–143.
- 33 J. Andersson, S. Areva, B. Spliethoff and M. Lindén, *Biomaterials*, 2005, **26**, 6827–6835.
- 34 F. Yao, J. P. LeGeros and R. Z. LeGeros, *Acta Biomater.*, 2009, **5**, 2169–2177.
- 35 R. Kumar, K. H. Prakash, P. Cheang and K. A. Khor, *Langmuir*, 2004, **20**, 5196–5200.
- 36 A. Peeters, E. A. P. De Maeyer, C. V. Alsenoy and R. M. H. Verbeeck, *J. Phys. Chem. B*, 1997, **101**, 3995–3998.
- 37 P. N. Gunawidjaja, I. Izquierdo-Barba, R. Mathew, K. Jansson, A. García, J. Grins, D. Arcos, M. Vallet-Regí and M. Edén, *J. Mater. Chem.*, 2012, **22**, 7214–7223.
- 38 Y. Y. Hu, X. P. Liu, X. Ma, A. Rawal, T. Prozorov, M. Akinc, S. K. Mallapragada and K. Schmidt-Rohr, *Chem. Mater.*, 2011, **23**, 2481–2490.
- 39 S. Liao, F. Watari, M. Uo, S. Ohkawa, K. Tamura, W. Wang and F. Cui, *J. Biomed. Mater. Res., Part B*, 2005, **74**, 817–821.
- 40 *Biomaterials*, ed. F. C. M. Driessens and R. M. H. Verbeeck, CRC Press, Boca Raton, 1990.

-
- 41 R. Wallayes, *Ann. Chim.*, 1952, **7**, 808–848.
42 D. Carlstrom, *Acta Radiol., Suppl.*, 1955, **121**, 1–59.
43 R. A. Young, *Clin. Orthop. Relat. Res.*, 1975, **113**, 249–262.
44 J. C. Elliott, *J. Appl. Crystallogr.*, 1980, **13**, 618–621.
45 J. C. Elliott, R. M. Wilson and S. E. P. Dowker, *Adv. X-Ray Anal.*, 2002, **45**, 172–181.
46 H. B. Lu, C. T. Campbell, D. J. Graham and B. D. Ratner, *Anal. Chem.*, 2000, **72**, 2886–2894.
47 M. Vallet-Regí and J. M. González-Calbet, *Prog. Solid State Chem.*, 2004, **32**, 1–31.
48 F. C. M. Driessens, *Ann. N. Y. Acad. Sci.*, 1988, **523**, 131–136.
49 S. V. Dorozhkin, *J. Mater. Sci.*, 2007, **42**, 1061–1095.
50 T. S. B. Narasaraaju and D. E. Phebe, *J. Mater. Sci.*, 1996, **31**, 1–21.
51 J. A. S. Bett, L. G. Christner and W. K. Hall, *J. Am. Chem. Soc.*, 1967, **89**, 5535–5541.
52 S. Hattar, A. Berdal, A. Asselin, S. Loty, D. C. Greenspan and J. M. Sautier, *Eur. Cells Mater.*, 2002, **4**, 61–69.
53 G. K. Hunter and H. A. Goldberg, *Proc. Natl. Acad. Sci. U. S. A.*, 1993, **90**, 8562–8565.
54 D. G. Reid, G. J. Jackson, M. J. Duer and A. L. Rodgers, *J. Urol.*, 2011, **185**, 725–730.
55 P. Layrolle and A. Lebugle, *Chem. Mater.*, 1994, **6**, 1996–2004.
56 A. George, L. Bannon, B. Sabsay, J. W. Dillon, J. Malone, A. Veis, N. A. Jenkins, D. J. Gilbert and N. G. Copeland, *J. Biol. Chem.*, 1996, **271**, 32869–32873.
57 J. Mahamid, A. Sharir, L. Addadi and S. Weiner, *Proc. Natl. Acad. Sci. U. S. A.*, 2008, **105**, 12748–12753.
58 E. Beniash, R. A. Metzler, R. S. K. Lam and P. U. P. A. Gilbert, *J. Struct. Biol.*, 2009, **166**, 133–143.
59 N. Temizel, G. Giriskan and A. C. Tas, *Mater. Sci. Eng., C*, 2011, **31**, 1136–1143.
60 J. D. Termine and E. D. Eanes, *Calcif. Tissue Res.*, 1972, **10**, 171–197.
61 F. Huang and J. F. Banfield, *J. Am. Chem. Soc.*, 2005, **127**, 4523–4529.
62 C. C. Chen, A. B. Herhold, C. S. Johnson and A. P. Alivisatos, *Science*, 1997, **276**, 398–401.